NUMERICAL SIMULATION OF SURFACE WATER WAVES ON THE SPHERE

Panayotis Panayotaros

Department of Mathematics

The University of Texas at Austin

Austin, TX 78712-1082

Abstract.

We present a scheme for the numerical simulation of small amplitude water waves in spherical geometry. The method is based on a free-surface potential flow model of water waves. The equations of motion have a Hamiltonian structure, are non-local and we use them to derive simpler small amplitude wave equations for water of arbitrary depth. In our simulation we consider such equations, and our numerical implementation preserves the Hamiltonian structure of the evolution. This fact is used to test the accuracy of the numerical integration and also in understanding some of the qualitative properties of small amplitude solutions. In particular, our observations suggest that the numerical solutions of the approximate equations are very accurate and that small solutions remain bounded.

1. Introduction

We describe a numerical scheme for simulating the motion of the free surface of a fluid layer surrounding a gravitating sphere.

Our investigation of this physical system is motivated by general questions on the dynamics of non-linear waves, and also by problems in geophysical flows, e.g. atmospheric tides. The main simplifying physical assumption we have made in modeling this system is that the flow inside the layer is potential. As potential free-surface flow is commonly used in studies of water waves (e.g. in the usual Euclidean geometry where the layer rests on a plane, see for instance [W], [L]), the numerical simulations we describe should be of wider interest.

Under the potential flow assumption, the evolution of the wave amplitude η (the radius of points in the surface) and the hydrodynamic potential at the free surface Φ completely determine the motion of the layer. Thus the dynamical quantities depend on two spatial variables. The trade-off is that the evolution equations for η and Φ are non-local and not given explicitly. They depend on the velocity at the free surface, and this quantity is obtained through solution of Laplace's equation, with boundary data Φ, in the domain occupied by the fluid, as determined by η.

One way past this obstacle is to derive approximate expressions for the velocity at the free surface. Using these expressions we can derive approximate water wave equations that can be investigated analytically or numerically. This is the classical approach, and the one that we follow here. (There is a long list of equations obtained this way: Korteweg-de Vries, Boussinesq, etc..) The main limitation of this approach is that the approximations assume that the amplitude and slope of the waves is small. Thus, our numerical investigation concerns small oscillations of the free surface of the spherical layer.

A more general approach, not discussed here, is to compute the velocity at the free surface (given η and Φ) numerically at each time-step, and then use the equations of motion to evolve η and Φ to the next time-step. Implementations of this general idea are in [LK] for 2-D periodic deep water waves, [PTM] for an axisymmetric waves on the sphere (see also [OM] for comparison between the two approaches).

Our numerical simulation of water waves on the sphere is distinguished by two features. First, we use an exact expression for the velocity at the surface (more precisely, its component normal to the surface) as an expansion in powers of the water wave amplitude. The terms in this expansion, viewed as linear operators on Φ, are pseudo-differential operators, and can be computed recursively to any desired order. Also, the fluid layer can be of arbitrary thickness. Analogous expressions have been used recently by several authors, in Euclidean geometry (see [GS], [GAS]). The improvement over earlier expressions for the surface velocity (see e.g. [W] ch. 8, [We], [DY]) is that we expand in the amplitude only, not in wavenumber, i.e. the expressions we use are uniform in wavenumber. We therefore expect that we can model a wider range of spatial scales using fewer terms in the expansion.

Another feature of our work, more important in the current implementation, is that the approximate water wave equations we will be integrating numerically are Hamiltonian systems. The Hamiltonian structure of the free surface potential flow was first derived by [Z] for deep water waves (see also [M]), and in a previous work (see [LP]), we adapted the Hamiltonian formulation of water waves to spherical geometry. The canonical variables are η and Φ and the Hamiltonian is the total energy of the fluid layer. As was noticed by [CG], [GAS], [R] and others, the velocity at the free surface is absorbed in the Hamiltonian. We can therefore use the expansions for the surface velocity discussed above so that all approximations of the surface velocity lead to corresponding approximate Hamiltonians. This way we obtain a hierarchy of water wave models that are automatically Hamiltonian systems. Here, we will consider truncations of the Hamiltonian in the wave amplitude and also in wavenumber, i.e. by setting all but a finite set of the spherical harmonic coefficients of η and Φ to zero. The resulting finite dimensional systems have the form of Hamilton's equations with the truncated Hamiltonian, and are solved numerically using an o.d.e. solver.

We saw several advantages in using the Hamiltonian formulation. We used energy conservation to assess the accuracy of the numerical integration, especially in cases where the numerical trajectories become unbounded. Also, the fact that the quadratic part of the Hamiltonian is positive-definite implies that for sufficiently small initial conditions, the solutions of the finite dimensional Galerkin systems should remain bounded for all time, in agreement with our numerical observations. We expect that the magnitude of the initial conditions leading to bounded solutions decreases as we increase the number if modes in the spectral truncation, which is also what we see. We note that in our simulations we did not use any artificial damping, in particular energy is conserved to high accuracy. This fact, together with comparison of the numerical trajectories of obtained through different methods suggest that we achieve high accuracy in the numerical integration.

The explicitly Hamiltonian implementation that we use in this paper relies on the Galerkin method and is fully spectral. Hence the code does not scale well as we increase the number of modes and the order in the wave amplitude. These problems can be addressed by using a fast spherical harmonic transform algorithms (see [DH]). In the pseudo-spectral method we solve the truncated equations of motion, not Hamilton's equations of motion for a truncated Hamiltonian. Since in many simulations energy conservation fails as the numerical trajectories become unbounded (see for instance [CS], [PTM], [DY]), an implementation that is explicitly Hamiltonian is a desirable first step.

The paper is organized as follows: in section 2 we outline the Hamiltonian formulation of the water wave problem and the expansion for the surface velocity. The discussion leads to the spectral (Galerkin) form of Hamilton's equations for water waves that we implement numerically. In Section 3 we discuss some practical issues related to the implementation of the equations in the computer, especially the production of the equations of motion on the sphere and size considerations. In section 4 we present and interpret the results of our numerical experiments. We discuss the accuracy of the numerical integration, energy conservation, bounded and unbounded numerical solutions, and we also present some comparisons of trajectories obtained through different spectral truncations, and through two different truncations in powers of the water wave amplitude.

2. Mathematical formulation

We consider a sphere of radius b and on top of it a layer of fluid ("sea" or "atmosphere") of thickness ("depth") h. Using the spherical coordinates r = radius, ϑ = polar, φ = azimuth, the surface of the layer will be the set of points with radius $r(\vartheta,\varphi)=\rho+\eta(\vartheta,\varphi)$, with $\rho = b + h$.

We are interested in the motions of the fluid layer. We will assume that the fluid is inviscid, incompressible, of uniform density ($=1$), and that the motion is irrotational (potential). For potential flow there exists a scalar ϕ, the hydrodynamic potential, so that the Eulerian velocity $\vec{u}$ is $\vec{u} = \nabla\phi$. For free surface potential flow, Euler's equations imply (see for instance [L]) that

(2.1)
$$\eta_t = \frac{\partial\phi}{\partial r} - \frac{1}{r^2}\frac{\partial\phi}{\partial\vartheta}\frac{\partial\eta}{\partial\vartheta} - \frac{1}{r^2\sin^2\vartheta}\frac{\partial\phi}{\partial\varphi}\frac{\partial\eta}{\partial\varphi} \quad ,$$

and

(2.2)
$$\phi_t = -\frac{1}{2}|\nabla\phi|^2 + \frac{K}{\rho+\eta} \quad ,$$

at the free surface,

(2.3)
$$\Delta\phi = 0$$

in the region occupied by the fluid, and

(2.4)
$$\frac{\partial\phi}{\partial r} = 0$$

at the bottom $r = b$.

Note that the evolution of the wave amplitude $\eta(\vartheta,\varphi)$ and the surface potential $\Phi(\varphi,\vartheta) = \phi(\varphi,\vartheta,\rho+\eta(\vartheta,\varphi))$ completely determine the evolution of the hydrodynamic potential ϕ inside the layer: at each instant the potential ϕ is the unique solution of the boundary value problem $\Delta\phi = 0$ inside the fluid layer, with $\phi = \Phi$ at the surface $r = \rho + \eta(\vartheta,\varphi)$ and $\frac{\partial\phi}{\partial r} = 0$ at $r = b$. Therefore, we can, in principle, rewrite (2.1)-(2.4) as evolution equations for η and Φ and reduce the spatial dimension of the evolving quantities by one. One complication is that such equations involve integral operators arising from the inversion of the Laplacian. Expressions for these operators in terms of

η and Φ will be approximate, and the evolution equations we will consider will be an approximation of (2.1)-(2.4).

In deriving approximate equations for the wave amplitude and surface potential, we will use the fact that the evolution equations (2.1)-(2.4) can be written in the form of Hamilton's equations. In particular, we will derive approximate equations that also have Hamiltonian structure. The idea is to start with the Hamiltonian of the full system and derive approximate equations by approximating the Hamiltonian. The terms involving the velocity at the free surface enter in our expression for the Hamiltonian.

The Hamiltonian formulation for water waves on the sphere is developed in [LP], here we only give an outline. The canonical variables are the surface elevation $\eta(\vartheta,\varphi)$ and the hydrodynamic potential at the surface $\Phi(\vartheta,\varphi)$. The Hamiltonian H is the total (kinetic + potential) energy of the system, namely

$$H = \frac{1}{2}\int_{S^2}\int_{r=b}^{r=\rho+\eta(\vartheta,\varphi)} |\nabla\phi|^2 dV + \int_{S^2}\int_{r=b}^{r=\rho+\eta(\vartheta,\varphi)} \left(-\frac{K}{r}\right) dV \quad . \tag{2.5}$$

The first integral corresponds to the kinetic energy and the second to the potential energy. Using Green's identity, we can also write

$$H = \frac{1}{2}\int_{S^2} \Phi R \frac{\partial\phi}{\partial n}\bigg|_{r=\rho+\eta(\vartheta,\varphi)} dA_r + \frac{1}{2}\int_{S^2}(-K)dA_r \quad . \tag{2.6}$$

Here $R = [1+(\frac{1}{r}\frac{\partial\eta}{\partial\vartheta})^2 + (\frac{1}{r\sin\vartheta}\frac{\partial\eta}{\partial\varphi})^2]^{\frac{1}{2}}$ and $\frac{\partial\phi}{\partial n}|_{r=\rho+\eta(\vartheta,\varphi)}$ is the normal derivative at the surface. We also use the notation $dA_r = r^2\sin\theta d\theta d\varphi$ with $r = \rho+\eta(\vartheta,\varphi)$. The quantity RdA_r is the area element of the free surface.

The Hamiltonian formulation of the water wave problem is the statement that the equations of motion (2.1)-(2.4) are equivalent to the equations

$$\eta_t = \left(\frac{\rho+\eta}{\rho}\right)^{-2}\frac{\delta H}{\delta\Phi} \quad , \quad \Phi_t = -\left(\frac{\rho+\eta}{\rho}\right)^{-2}\frac{\delta H}{\delta\eta} \quad . \tag{2.7}$$

The variational derivative $\frac{\delta F}{\delta x}$ is defined by $<\frac{\delta F}{\delta x},\delta x>= F'$, where F' is the Frèchet derivative of F with respect to x, and $<,>$ is the L^2 inner product on S^2 (with radius ρ).

Equations (2.7) are Hamilton's equations with a "non-canonical" Poisson bracket (see for instance [D], ch.1). It will be convenient to write Hamilton's equations (2.7) in the "diagonalized form", i.e. without the prefactor $\left(\frac{\rho+\eta}{\rho}\right)^{-2}$, by using the variables ($\tilde{\eta}$, $\tilde{\Phi}$) defined by

$$\tilde{\eta} = \eta\left(1+\frac{\eta}{2\rho}\right) \quad , \quad \tilde{\Phi} = \Phi\left(1+\frac{\eta}{\rho}\right) \quad . \tag{2.8}$$

Considering the basis of spherical harmonics $Y_\gamma(\vartheta,\varphi)$, with $\gamma = [l,m]$, $l = 1,2,\ldots$, $m = -l,\ldots,l$ (e.g. see [McR]), we have $\eta = \sum_\gamma \eta_\gamma Y_\gamma$, $\Phi = \sum_\gamma \Phi_\gamma Y_\gamma$, and Hamilton's equations become, after the transformation of (2.8),

$$\frac{d\tilde{\eta}_\gamma}{dt} = \frac{\partial H}{\partial \tilde{\Phi}^*_\gamma} \quad , \quad \frac{d\tilde{\Phi}_\gamma}{dt} = -\frac{\partial H}{\partial \tilde{\eta}^*_\gamma} \quad . \tag{2.9}$$

To write the Hamiltonian explicitly in terms of the canonical variables we first define the Dirichlet-Neumann operator $G(\eta)\Phi$ by

$$G(\eta)\Phi = R\frac{\partial\phi}{\partial n}\bigg|_{r=\rho+\eta(\vartheta,\varphi)} \quad . \tag{2.10}$$

¿From (2.6) we have

$$H = \frac{1}{2}\int_{S^2} \Phi G(\eta)\Phi dA_r + \frac{1}{2}\int_{S^2} (-K) dA_r \quad , \tag{2.11}$$

and we look for an expression for $G(\eta)\Phi$. The operator $G(\eta)\Phi$ relates the Dirichlet data at the free surface to Neumann data after inverting the Laplacian, and is linear in Φ and non-linear in η. Expressions for $G(\eta)\Phi$ can be derived by assuming that we can write an expansion $G(\eta) = \sum_{i=0}^{\infty} G_i(\eta)$ with the $G_i(\eta)$ homogeneous of order i in η. Using the method described in [LP], we compute $G_0(\eta)$, ..., $G_{i-1}(\eta)$. For instance, we have

$$G_0(\eta)Y_\gamma = \frac{1}{u_\gamma(\rho)} u_\gamma{}'(\rho) Y_\gamma \quad , \tag{2.12}$$

$$\begin{aligned} &G_1(\eta)Y_\gamma = \\ &= \frac{1}{u_\gamma(\rho)}\left[\eta u_\gamma{}''(\rho)Y_\gamma - \frac{1}{\rho^2}u_\gamma(\rho)\left[\eta_\vartheta \frac{\partial Y_\gamma}{\partial\vartheta} + \frac{1}{\sin^2\vartheta}\eta_\varphi \frac{\partial Y_\gamma}{\partial\varphi}\right] - G_0(\eta)\eta u_\gamma{}'(\rho) Y_\gamma\right] \quad . \end{aligned} \tag{2.13}$$

Higher order terms can be readily computed recursively, each $G_i(\eta)$ is given in terms of $G_0(\eta)$, ..., $G_{i-1}(\eta)$. The $G_i(\eta)\phi$ are specified by their action on the spherical harmonic coefficients Φ_γ and and can be thought of as pseudo-differential operators. We remark that in case of water waves in $\mathbf{R}^2$ and $\mathbf{R}^3$, analogous expansions of $G(\eta)\Phi$ are shown to converge, as a linear operator $W^{s+1,q} \to W^{s,q}$ for η in C^{s+1} and of sufficiently small C^1 norm (see [CM], [GSS] for precise statements and proof in the 2-D and 3-D case respectively).

¿From (2.11), the expansion of $G_i(\eta)\phi$ gives us an expansion for the Hamiltonian H, i.e. $H = H_0 + H_1 + H_2 + \ldots$ with $H_0 = \frac{1}{2}\int \Phi G_0(\eta)\Phi + \frac{1}{2}\int g\eta^2$, $H_1 = \frac{1}{2}\int \Phi G_1(\eta)\Phi$ and so on. The H_k are of order $k+2$ in the canonical variables. Approximate water wave models are derived by considering the Hamiltonian up to some H_k and using Hamilton's equations of motion (2.8).

Using the spectral variables $\tilde{\eta}_\gamma$, $\tilde{\Phi}_\gamma$ (and dropping the tilde from now on) we have the Hamiltonian $H = H_0 + H_1 + \ldots$ with

$$H_0 = \frac{1}{2}\rho^2 \sum_\gamma \frac{u_\gamma{}'(\rho)}{u_\gamma(\rho)} \Phi_\gamma \Phi_\gamma^* + \frac{1}{2}\rho^2 \sum_\gamma g\eta_\gamma \eta_\gamma^* \quad , \tag{2.14}$$

$$\begin{aligned} H_1 = \frac{1}{2}\rho^2 \sum_{\gamma_1,\gamma_2,\gamma_3} \left(\frac{u''_{\gamma_2}(\rho)}{u_{\gamma_2}(\rho)} - \frac{u'_{\gamma_1}(\rho)}{u_{\gamma_1}(\rho)} \frac{u'_{\gamma_2}(\rho)}{u_{\gamma_2}(\rho)} \right) \Phi_{\gamma_1} \Phi_{\gamma_2} \eta_{\gamma_3} \int Y_{\gamma_1} Y_{\gamma_2} Y_{\gamma_3} \\ + \frac{1}{2} \sum_{\gamma_1,\gamma_2,\gamma_3} \Phi_{\gamma_1} \Phi_{\gamma_2} \eta_{\gamma_3} \int Y_{\gamma_1} \nabla Y_{\gamma_2} \cdot \nabla Y_{\gamma_3} \quad , \end{aligned} \tag{2.15}$$

and Hamilton's equations

$$\dot{\eta}_\gamma = \frac{\partial H}{\partial \Phi_\gamma^*} \quad , \quad \dot{\Phi}_\gamma = -\frac{\partial H}{\partial \eta_\gamma^*} \quad . \tag{2.16}$$

The above expressions for the Hamiltonian and the Hamilton's equations (2.16) are the basis of our numerical implementation using the spectral method.

Note the we have only included the quadratic part of the gravitational potential energy, so that all the non-linear terms in the equations of motion arise from the kinetic energy. Also, if we use dimensionless variables with $\eta^* = \frac{\eta}{A}$, A a typical wave amplitude, and $\varepsilon = \frac{A}{h}$, $\beta = \frac{h}{b}$, we have $G_j(\eta) \sim (\varepsilon\beta)^j G_j(\eta^*)$. Thus by considering $H = H_0 + H_1$ we assume that $\varepsilon\beta$ is small. In the simulations we fixed β and considered ε in a range near 0.05. Although physically the use of the cubic Hamiltonian becomes better justified for even smaller ε, the above range was interesting because it was where the numerical solutions would become to become unbounded (for the set of initial conditions we used).

3. Numerical implementation

We will now describe in some detail the generation of the Galerkin truncations of the equations (2.14)-(2.16), and the numerical integration method we used.

We consider the Hamiltonian $H = H_0 + H_1$ of (2.14)-(2.16) and truncate it in wavenumber by considering summations over a finite set of indices γ. Here we are interested in truncations that include all modes with $\gamma = [l, m]$ s.t $l \le l_{max}$.

To write the equations of motion we need to evaluate the Hamiltonian H_1 (producing the linear equations is straightforward), and in particular the triple integrals $\int Y_{\gamma_1} Y_{\gamma_2} Y_{\gamma_3}$ and $\int Y_{\gamma_1} \nabla Y_{\gamma_2} \cdot \nabla Y_{\gamma_3}$ of spherical harmonics. Using the definition of the harmonics $Y_\gamma = Y_l^m(\vartheta, \varphi) = e^{im\varphi} P_l^{|m|}(\mu)$ with $\mu = \cos\vartheta$ and $P_l^m(\mu)$ the associated Legendre functions (see ,e.g., [BL], [McR]), we have

$$\int Y_{\gamma_1} Y_{\gamma_2} Y_{\gamma_3} = \delta_{123} \int_{-1}^{1} P_{\gamma_1} P_{\gamma_2} P_{\gamma_3} d\mu \tag{3.1}$$

and

$$\int Y_{\gamma_1} \nabla Y_{\gamma_2} \cdot \nabla Y_{\gamma_3} = \delta_{123} \int_{-1}^{1} \left[(1-\mu^2) P_{\gamma_1} \frac{dP_{\gamma_2}}{d\mu} \frac{dP_{\gamma_3}}{d\mu} - \frac{m_2 m_3}{1-\mu^2} P_{\gamma_1} P_{\gamma_2} P_{\gamma_3} \right] d\mu \tag{3.2}$$

with $\delta_{123} = \int_0^{2\pi} e^{i\left(\sum_{i=1}^{3} m_i\right)\varphi} d\varphi$. We evaluated the triple integrals of the associated Legendre functions up to some $\gamma = [l, m]$ with $l \le l_{max}$ using a Maxima program. The generation of the Legendre functions and the indefinite integration were performed symbolically and hence was not affected by round-off or numerical error. Note that the triple integrals of (3.1), (3.2) vanish unless $|l_1 - l_2| \le l_3 \le l_1 + l_2$, and $l_1 + l_2 + l_3$ is even. These "selection rules" can be used to check and speed-up the evaluation of the integrals. Another check is afforded by known formulas for the triple integrals of harmonics, see for instance [BL]. We found that the computer evaluation is more efficient for calculating the triple integrals than the formulas.

To produce the equations of motion it is convenient to define the variables a_γ, a_γ^* by

$$\eta_\gamma = \frac{\sqrt{2}}{2} \sqrt{\frac{\omega_\gamma}{g}} (a_\gamma + a_{\bar{\gamma}}^*) \quad , \quad \Phi_\gamma = -i \frac{\sqrt{2}}{2} \sqrt{\frac{g}{\omega_\gamma}} (a_\gamma - a_{\bar{\gamma}}^*) \tag{3.3}$$

where if $\gamma = [l,m]$ then $\overline{\gamma} = [l,-m]$. Since η and Φ are real, we have $\eta^*_{[l,m]} = \eta_{[l,-m]}$, $\Phi^*_{[l,m]} = \Phi_{[l,-m]}$ and (3.3) defines the a_γ uniquely. The Hamiltonian, truncated to cubic terms, takes the form

$$H_0 = \sum_\gamma \omega_\gamma a_\gamma a^*_\gamma \quad , \quad \omega^2(\gamma) = \frac{u_\gamma{}'(\rho)}{u_\gamma(\rho)} \tag{3.4}$$

$$H_1 = \sum_{\gamma_1,\gamma_2,\gamma_3} (A_{\gamma_1\gamma_2\gamma_3} a_{\gamma_1} a_{\gamma_2} a_{\gamma_3} + B_{\gamma_1\gamma_2\gamma_3} a_{\gamma_1} a_{\gamma_2} a^*_{\gamma_3}) + c.c. \tag{3.5}$$

with

$$A_{\gamma_1\gamma_2\gamma_3} = -\frac{\sqrt{2}}{4}\sqrt{\frac{\omega_{\gamma_2}}{\omega_{\gamma_1}\omega_{\gamma_3}}} I_{\gamma_1\gamma_2\gamma_3} \quad , \tag{3.6}$$

$$B_{\gamma_1\gamma_2\gamma_3} = -\frac{\sqrt{2}}{4}\left(-\sqrt{\frac{\omega_{\gamma_2}}{\omega_{\gamma_1}\omega_{\gamma_3}}} I_{\overline{\gamma}_3\gamma_1\gamma_2} - \sqrt{\frac{\omega_{\gamma_2}}{\omega_{\gamma_1}\omega_{\gamma_3}}} I_{\gamma_1\overline{\gamma}_3\gamma_2} + \sqrt{\frac{\omega_{\gamma_3}}{\omega_{\gamma_1}\omega_{\gamma_2}}} I_{\gamma_1\gamma_2\overline{\gamma}_3}\right) \quad , \tag{3.7}$$

and with the $I_{\gamma_1\gamma_2\gamma_3}$ are defined by $H_1 = \sum_{\gamma_1\gamma_2\gamma_3} I_{\gamma_1\gamma_2\gamma_3} \Phi_{\gamma_1}\Phi_{\gamma_2}\eta_{\gamma_3}$ and (2.15). Using the calculated values of the triple integrals, we produce and store the $A_{\gamma_1\gamma_2\gamma_3}$ and $B_{\gamma_1\gamma_2\gamma_3}$. Using the real variables q_γ, p_γ defined by $a_\gamma = q_\gamma + ip_\gamma$, for each triple of γ_1, γ_2, γ_3 we produce the Hamiltonian and the equations using Hamilton's equations

$$\dot{q}_\gamma = \frac{1}{2}\frac{\partial H}{\partial p_\gamma} \quad , \quad \dot{p}_\gamma = -\frac{1}{2}\frac{\partial H}{\partial q_\gamma} \quad . \tag{3.8}$$

For a truncation of up to $l = l_{max}$ we have a system of $N = 2(l^2_{max} + 2l_{max})$ equations. The length of the equations, i.e. the number of monomials produced by the above procedure is $O(N^{\frac{5}{2}})$: $O(N^3)$ terms from the cubic Hamiltonian H_1, reduced by the "selection rules" $m_1 + m_2 \pm m_3 = 0$. For a Hamiltonian of order k the length of the equations is $O(N^{k-\frac{1}{2}})$. (Also of interest are the axisymmetric solutions with $O(l^k)$ terms.) Since the evaluation of the equations at each time step is the main computational cost of of the numerical integration, (in the best cases, for we may also need to evaluate the Jacobian), the rapid increase of the length of the equation with wavenumber and especially with the order of the Hamiltonian is the major drawback of our numerical implementation using the spectral method. This problem is usually addressed using pseudo-spectral method, where the length of the equation for a Hamiltonian of order $k+1$ will be $O(kN)$. However, the pseudo-spectral method does not preserve the Hamiltonian structure of the model equations.

In producing the equations of motion, the most time consuming step is the calculation of the triple integrals of harmonics with Maxima. For $l_{max} = 10$, this computation took about 36 hrs. (on a Sun Sparc20). However, the code we have at present can be optimized considerably. The evaluations of the coefficients of the cubic Hamiltonian for $l_{max} = 8$, also using Maxima, took 2 hrs. and the production of equation using Fortran took a few minutes. The compilation of the equations of motion for $l_{max} = 8$ took about 40 min. In general, Maxima runs very slowly compared to Fortran, and the procedure can become more efficient simply by writing all code in Fortran. Of-course the above are one-time costs and are not as important as the efficiency of integration. Moreover, the symbolic evaluation of the triple integrals is exact. Note that the higher order terms of the Hamiltonian i.e. H_2, H_3, etc., involve integrals of four and more spherical harmonics (see [LP]). However, all these multiple integrals can be reduced to the triple integrals we have already computed, thus higher order Hamiltonians can be evaluated quite efficiently.

In evaluating the Hamiltonian, we set the radius b of the sphere to $b = 1$. The depth parameter $\rho = b + h$ (h is the thickness of the layer), which enters in the Hamiltonian is set to some value before evaluating the Hamiltonian, so that to use a different value of ρ we need to produce the equations anew. In the calculations below, we set $\rho = 1.2$. Although it would be desirable to leave ρ as a free parameter in the equations of motion, because of the relatively complicated nature of the dependence of the coefficients of the Hamiltonian on ρ, pre-evaluating the coefficients that depend on ρ makes the integration more efficient.

To integrate the equation we have used LSODE, a Fortran numerical integration package available through netlib. The algorithms in LSODE are described in [H]. The first integration algorithm we used, referred hereafter as the Adams method, is a predictor-corrector multi-step method, where the prediction step is performed by an (explicit) Adams-Bashforth formula, and the correction step is done by an (implicit) Adams-Moulton formula. (see, for instance, [I], ch.2). The corrected value is computed by (Picard) iteration. The second algorithm that we chose is based on the backward differentiation formulas (BDF) (see [I], ch.2). The BDF formulas give a multi-step implicit method employing Newton iteration. The BDF method is used mainly for stiff systems. In LSODE, both the Adams and BDF methods run with variable time-step and order. The choice of step size and order is performed automatically during the integration so that the computed values of q_γ, p_γ are within a user specified local error tolerance. The formulas for the estimation of the local error and the decision tree for changing the step-size and the order can be found in [G] p.155 (see also [SG] for the Adams method, but the procedures are the same for the BDF method).

4. Results

In the numerical experiments, we first evaluate the accuracy of the numerical integration by using energy conservation and by comparing the results different integration methods and integration parameters. We then compare the numerical trajectories obtained through different truncations and comment on the boundedness of the numerical solution and the error in ignoring higher order terms in the Hamiltonian.

To test the integration we considered the equation with $l_{max} = 8$. Rescaling the variables a_γ as $a_\gamma = \epsilon \tilde{a}_\gamma$ with $\tilde{a}_\gamma \approx O(1)$ (and dropping the tilde form the notation), the Hamiltonian becomes $H_0 + \epsilon H_1$ and we vary the magnitude of the initial conditions by varying ϵ.

We use energy conservation as a benchmark and also compare the output for different error tolerances and methods, Adams and BDF. Our observations can be summarized as follows (a more quantitative account is given later):

i) For sufficiently small initial conditions (or ϵ) the solutions stay bounded up to the time we integrated. For larger initial conditions the solutions "blow-up", more precisely, most modes grow from $<< 1$ to $> O(1)$, and at some point, their time derivatives grow abruptly to large values and the integration halts. Varying the error tolerance and integration algorithm, boundedness or blow-up for given initial conditions persists. Note that, since the Hamiltonian is positive definite near the origin, small solutions are expected to stay bounded.

ii) For both methods, energy is conserved to an accuracy that increases as we decrease the error tolerance. The accuracy of energy conservation also decreases slightly as we integrate over longer times. Energy conservation is observed regardless of whether the trajectories stay bounded or not.

iii) The graphs of the numerical $q_\gamma(t)$, $p_\gamma(t)$ obtained through different methods and error tolerances agree quantitatively for both bounded and unbounded solutions.

We remark that, in our runs, the BDF method is ~ 40 times slower than the Adams method (since the BDF also requires evaluation of the Jacobian), and that comparison between the two methods is over rather small time intervals.

In a first series of runs, we used the Adams method and considered values of the error tolerance w in the range $w = 10^{-5}$ to 10^{-15}. Also ϵ was in the range 0.01 to 0.1. Typical accuracy in energy conservation is indicated in Tables 1, 2 and 3. Tables 2 and 3 correspond to solutions that eventually blow-up. Typically we see that for $w = 10^{-5}$, 10^{-9}, 10^{-15} energy is conserved to $\sim 3, 8, 13$ significant digits over $\Delta t = 20 \times 0.05$, and $\sim 2, 6, 12$ over $\Delta t = 500 \times 0.05$. Near the blow-up we also see energy conservation, but with a slight decrease in accuracy for given error tolerance, see Tables 2, 3. Note that for large amplitudes, it is possible to lose accuracy in energy conservation without losing accuracy in the numerical solutions. If, for instance, all the computed modes are w-close to their real values, the error in the computed value of the Hamiltonian is estimated above by $2M_0 a w + 3M_1 a^2 w + O(w^2)$, where M_0, M_1 = number of quadratic and cubic terms in the Hamiltonian respectively, and a is the largest amplitude of all the modes. Comparing the trajectories of the modes for different error tolerances we see good agreement, see for instance Figures 1, 2 and 3 (from the experiments of Tables 1, 2, 3 resp.). Small discrepancies are noticeable, but the graphs obtained for $E = 10^{-9}$, 10^{-15} are practically indistinguishable. Note that this agreement is also observed near the blow-up.

In a another series of runs the procedure was repeated using the BDF method. The more systematic observations concern smaller time intervals. Over a time interval $\Delta t = 20 \times 0.05$, accuracy in energy conservation is as in the Adams method, see for example Tables 3, 4. During the blow-up we observe the same loss of accuracy in energy conservation as with the Adams method. Table 3 and 4 refer to the same experiment with the Adams and BDF method respectively

We have also compared the Adams and BDF methods for given error tolerances, over time intervals $\Delta t = 50 \times 0.05$ (and longer ones but less systematically). We observe that the trajectories of the modes agree to the accuracies of energy conservation (± 1 decimal). See for instance Table 5. Any discrepancies are too small to notice in the graphs of Fig. 3, 5.

¿From the above we may conclude that the integration using both methods is faithful to the equations of motion and that we can achieve high accuracy. Unbounded solutions do not seem to be due to any numerical instabilities, since energy is conserved and different methods and error tolerances give similar results up to accuracy. For sufficiently small initial conditions solutions stay bounded, while for larger initial conditions they start to increase without bound. Both behaviors are consistent with the Hamiltonian consisting of a positive definite quadratic a cubic part (we further remarks on this later). Note that, near the "blow-up", we see rapid increase in magnitude of the derivatives of the modes, and we may also have some loss of accuracy in the integration as interpolated values of higher derivatives that are used to estimate the error (see [G], p.155) may underestimate it.

We also see that the much more efficient Adams method performs equally well as the BDF method. It should be noted that the equations of motion are not expected to be stiff for small trajectories. Here, a Hamiltonian system is defined to be stiff, if one of the eigenvalues of the the time-1 map of the variational equation along some trajectory has modulus $>> 1$. For the equations we are considering, near the origin, the eigenvalues of such maps are $\epsilon-$close to the unit circle.

To compare the trajectories obtained using truncations with $l_{max} = 8, 4$ we have considered monochromatic initial conditions i.e. with $a_\Gamma = c_\Gamma$, $a_\gamma = 0$ if $\gamma \neq \Gamma$ (also Γ has $l < 4$). In the comparisons below, we have used the Adams method with error tolerance 10^{-9}.

For some initial conditions (with c_Γ between 0.05 and 0.3, depending on Γ) the trajectories of the $l_{max} = 8$ truncation become unbounded, while the $l_{max} = 4$ trajectories remain bounded. For larger initial conditions both truncations lead to unbounded trajectories, while for smaller initial conditions both truncations lead to bounded solutions.

For initial conditions where both truncations have bounded trajectories , we observe the common pattern that the "dominant" mode (the one that is initially non-zero) oscillates with an amplitude modulation that is within $10^{-2}-10^{-1}c_\Gamma$. The other modes, oscillate irregularly but with small amplitude, within $10^{-2}-10^{-1}$. For both truncations, the modulation of the dominant mode and the amplitude of the other modes increases with c_Γ. Typical mode trajectories are shown in Fig. 6 and 7. Generally, the modulation of the dominant mode is markedly larger in the $l_{max}=8$ truncation, by a factor $10^{-2}-10^{-1}$, depending on the initial amplitude.

For the case of initial conditions that lead to unbounded trajectories with the $l_{max}=8$ truncation only, comparing the trajectories before the blow-up, we see an even larger amplitude modulation of the dominant mode in the $l_{max}=8$ truncation (around $0.2c$) and a larger discrepancy between the modulation of the dominant mode in the two truncations. Thus for such initial conditions, the discrepancy of between the two truncations is appreciable even before the blow-up stage.

We make some further remarks on the boundedness of solutions. Considering the spectral truncations of Hamilton's equations for the Hamiltonian $H=H_0+H_1$ as an o.d.e. in $\mathbf{R}^N$, to show that small initial data remain bounded, it suffices to find $0<c<1$ and $\tilde{c}$, $\delta>0$ so that

$$cH_0(x)<H(x)<\tilde{c}H_0(x) \quad , \quad \forall x\in\mathbf{R}^N \quad \text{s.t.} \quad H_0(a)<\delta \quad . \tag{4.1}$$

Here the quadratic Hamiltonian H_0 is positive definite and can used as the (square of the) norm in $\mathbf{R}^N$. From (4.1) it follows that there exists $\delta'<\delta$ so that for any trajectory $x(t)$ with initial condition $x(0)$ s.t. $H_0(x(0))<\delta'$ will satisfy $H_0(x(t))<\delta$ for all time. Since H_1 is cubic such c, $\tilde{c}$ and δ can always be found, if we choose δ sufficiently small. Note that δ will not be uniform in the dimension N, it will be $\delta\sim\frac{1}{N^3}$. Note that this is a rough estimate, but an estimate that is uniform in N does not seem to exist.

The boundedness of solutions for small initial data also allows us to make a short time estimate of the error in ignoring the terms that arise from the quartic part of the Hamiltonian. For a fixed truncation in the wavenumber, we can compare the solutions of (i) $\dot{x}=f(x)$ denoting the equation obtained using the quadratic and cubic Hamiltonian and (ii) $\dot{y}=f(y)+g(y)$ obtained by adding the terms from the quartic Hamiltonian. These are o.d.e.s in $\mathbf{R}^N$. For both equations, small initial conditions lead to bounded trajectories and we now combine these statements for the two equations. It is also convenient to restate boundedness using a norm that is different from the energy norm used previously. In particular, let ω_0, ω_M be the frequencies of the modes with $l=0$,

$l = l_{max}$ respectively, and $I_{3,M}$, $I_{4,M}$ be the absolute value of the largest term in the cubic and quartic part of the Hamiltonian respectively. Also let $|x| = |x_1| + \ldots + |x_N|$ for $x \in \mathbf{R}^N$. Then for $c_A = \frac{\omega_0}{N I_{3,M}}$ we have found that

$$|z(0)| < \sqrt{\frac{\omega_0}{40\omega_M N}} c_A \tag{4.2}$$

implies

$$|z(t)| < \frac{c_A}{\sqrt{2}} \quad , \quad \forall t \geq 0 \quad , \tag{4.3}$$

where $z(t)$ can be either of $x(t)$ or $y(t)$. Note that c_A was chosen so that for $|z| < c_A$ we have $\frac{1}{2}H_0 < H < 10H_0$, where H can be either the cubic or the quartic Hamiltonian. We can use (4.3) to bound K, the supremum of $|g(y(t))|$ over $t \geq 0$ and also L, a number satisfying $|f(x(t)) - f(y(t))| < L|x(t) - y(t)|$ for all $t \geq 0$. Namely, we have computed

$$L < 2N\omega_M \quad , \quad K < I_{4,M}(c_A)^3 \quad . \tag{4.4}$$

Then for initial conditions $x(0) = y(0)$ satisfying (4.2) (with z(0) = x(0)), we use Gronwall's inequality to estimate the difference $\zeta(t) = x(t) - y(t)$ by

$$|\zeta(t)| < I_{4,M}(c_A)^3 \frac{e^{2\omega_M N t}}{2\omega_M N t} \quad , \quad \forall t \geq 0 \quad . \tag{4.5}$$

Clearly, (4.5) is useful only for short time, e.g. $t \sim \frac{1}{2\omega_M N}$. For longer time, $|\zeta(t)| < \sqrt{2}c_A$ from (4.3) becomes stronger than (4.5).

We remark that a statement like (4.5) is best used to investigate the robustness under addition of extra terms of specific motions of the equation $\dot{x} = f(x)$, e.g. periodic solutions of $\dot{x} = f(x)$. On the other hand, even without a detailed knowledge of the dynamics of $\dot{x} = f(x)$, our numerical observations suggest that for some special initial conditions the estimates of K and L can be improved (but on a heuristic, not rigorous basis at this point). For instance, for a monochromatic initial condition, e.g. with wavenumber $l = l_S$ and S small, that stays nearly monochromatic in both quadratic and cubic equations, (for the quadratic non-linearity such solutions were observed), L is approximately bounded by $2\omega_S$. If the initial amplitude is sufficiently small, $|\zeta(t)|$ can be smaller, e.g. by an order of magnitude, than $\sqrt{2}c_A$ for a small multiple of periods $\frac{2\pi}{\omega_S}$ of the linearized motion of the mode.

5. Conclusion

We have presented a method to simulate water waves of small amplitude in spherical geometry, using explicit expressions of the Dirichlet-Neumann operator and utilizing the Hamiltonian structure of the water wave problem. The spatial truncation of the equations of motion preserves the Hamiltonian structure of the full problem. This fact allows us to better check the accuracy of the numerical integration, and can also be used to show that, for sufficiently small initial data, solutions should stay bounded. From our numerical observations we conclude that the numerical trajectories are accurate and that small amplitude solutions stay bounded long times, without the introduction of artificial damping.

A known problem with the Galerkin method is that the o.d.e. we solve numerically can be very large. We believe that, at least the storage of the equation can be optimized significantly. In view of the advantages of our approach, it is worthwhile to push in the direction of including the quartic Hamiltonian or more modes. One idea is to use normal form theory to eliminate non-resonant terms in the Hamiltonian by canonical transformations. Our formal calculations suggest that the transformed equations scale much better as we include higher order terms and more modes.

6. Acknowledgments

I would like to thank Prof. de la Llave for valuable discussions on this work. Part of the research reported in this paper was supported by an NSF grant.

7. REFERENCES

[BL] L.C. Biedenharn, J.D. Louck: Angular momentum in quantum physics-theory and application, Addison-Wesley, Reading, Mass. (1981)

[CG] W. Craig, M.D. Groves: Hamiltonian long-wave approximation to the water wave problem, Wave Motion 19, 367-389 (1994)

[CM] R.R. Coifman, Y. Meyer: Non-linear harmonic analysis and analytic dependence, AMS Proc. Symp. Pure Math. 43, 71-78 (1985)

[CS] W. Craig, C. Sulem: Numerical simulation of gravity waves, Jour. Comp. Phys. 108, 73-83 (1993)

[CSS] W. Craig, U. Schanz, C. Sulem: The modulational regime of three-dimensional water waves and the Davey-Stewartson system, preprint (1995)

[D] B.A. Dubrovin: Geometry of Hamiltonian evolutionary systems, Bibliopolis, Napoli (1991)

[DH] J.R. Driscoll, D.M. Healy Jr.: Computing Fourier transforms and convolutions on the 2-sphere, Adv. Appl. Math. 15, 202-250 (1994)

[DY] D.G. Dommermuth, D. K. P. Yue: A high order spectral method for the study of non-linear gravity waves, Jour. Fluid Mech. 184, 267-288 (1987)

[G] W. Gear: Numerical initial value problems in ordinary differential equations, Prentice Hall, Englewood Cliffs, New Jersey (1971)

[GAS] M. Glozman, Y. Agnon, M. Stiassnie: High order formulation of the water wave problem, Physica D 66, 347-367 (1993)

[H] A. C. Hindmarsh: Odepack, a systematized collection of ode solvers, in Scientific computing, ed. S. S. Stepleman et al., North-Holland, Amsterdam, 55-64 (1983)

[I] A. Iserles: A first course in the Numerical Analysis of differential equations, Cambridge Univ. Press, Cambridge (1996)

[L] H. Lamb: Hydrodynamics, Dover, New York (1932)

[LP] R. de la Llave, P. Panayotaros: Water waves on the surface of the sphere, Jour. Nonlinear Sci. 6, 147-167 (1996)

[M] J.W. Miles: On Hamilton's principle for surface waves, Jour. Fluid Mech. 83, 153-158 (1977)

[McR] T.M. MacRoberts: Spherical harmonics, Pergamon Press, London (1967)

[OM] H. S. Ölmez, J. H. Milgram: Numerical methods for nonlinear interactions between water waves, J. Comp. Phys. 118, 62-72 (1995)

[PTM] N.A. Pelekasis, J.A. Tsamopoulos, G.D. Manolis: A hybrid finite-boundary element method for inviscid flows with free surface, Jour. Comp. Phys. 101, 231-251 (1992)

[SG] L.F. Shampine,M. K. Gordon: Computer solution of ordinary differential equations: the initial value problem, Freeman, San Francisco (1975)

[We] B. J. West: Statistical properties of water waves. Part I., J. Fluid Mechanics 117, 187-210 (1982)

[Z] V.E. Zakharov: Stability of periodic waves of finite amplitude on the surface of a deep fluid, Jour. Appl. Tech. Phys. 2, 190-194 (1968)

8. Captions

Tables 1-3: energy conservation for different tolerances, Adams method.

Table 4: energy conservation for different tolerances, BDF method, same experiment as in Table 3.

Fig. 1a: mode $q(2,-2)$, error tolerance $\sigma = 10^{-5}$, 10^{-15}. The values are indistinguishable at this resolution in the picture (n = number of timesteps). Energy in Table 1.

Fig. 1b: detail from Fig. 1a, small discrepancy for the two different error tolerances is now resolved.

Fig. 2a: mode $q(6,0)$, blow-up at $n \approx 735$, error tolerance $w = 10^{-15}$. Energy in Table 2.

Fig. 2b: mode $p(6,0)$ near blow-up at $n \approx 735$, error tolerances $w = 10^{-5}$, 10^{-15}.

Fig. 2c: mode $p(3,0)$ blow-up at $n \approx 735$, error tolerances $w = 10^{-5}$, 10^{-15}.

Fig. 3a: mode $p(2,2)$, blow-up at $n \approx 41$, error tolerances $w = 10^{-9}$, 10^{-15}, indistinguishable at this resolution in the picture. Energy in Table 3.

Fig. 3b: mode $p(7,-6)$, blow-up at $n \approx 41$, error tolerances $w = 10^{-9}$, 10^{-15}, difference indistinguishable at this resolution in the picture.

Fig. 4: mode $p(7,-6)$ Adams-BDF comparison, error tolerances $w = 10^{-15}$, difference indistinguishable at this resolution in the picture. Energy in Table 3 (Adams), Table 4 (BDF).

Fig. 5a-f: shape of the free surface. The radius here is the polar angle, and the angle is the azimuth. The center and the edge of the disk are the north and south pole on the sphere. The pictures are from the experiment of Fig. 2. At about $n = 690$ a peak develops at the south pole. It become sharper and its height increases, until the integration halts.

Fig. 6a: evolution of the mode $p(3,0)$ for truncations with $l_{max} = 8$, 4. Initially all other modes are set to zero.

Fig. 6b: evolution of the mode $p(4,0)$ for truncations with $l_{max} = 8,\ 4$.

Fig. 7a: evolution of the mode $p(3,3)$ for truncations with $l_{max} = 8,\ 4$. Initially all other modes are set to zero.

Fig. 7b: evolution of the mode $p(4,4)$ for truncations with $l_{max} = 8,\ 4$.

Energy Conservation - Table 1			
n*	$Error$† $= 10^{-5}$	10^{-9}	10^{-15}
0	$Energy = 1.1327$	1.1327044	1.1327044645353
10	1.1329	1.1327044	1.1327044645358
20	1.1331	1.1327044	1.1327044645358
100	1.1341	1.1327045	1.1327044645359
200	1.1365	1.1327044	1.1327044645360
400	1.1392	1.1327041	1.1327044645362
500	1.1408	1.1327039	1.1327044645359

* $n = \#$ of time-steps, $t = n \times 0.05$
† $Error$ = local error tolerance

Energy Conservation - Table 2			
n*	$Error$† $= 10^{-5}$	10^{-9}	10^{-15}
0	$Energy = 1.129$	1.1293332	1.12933323854
10	1.129	1.1293332	1.12933323854
20	1.129	1.1293332	1.12933323854
200	1.133	1.1293333	1.12933323854
500	1.141	1.1293331	1.12933323854
700	1.147	1.1293330	1.12933323854
720	1.148	1.1293330	1.12933323854
730	1.148	1.1293333	1.12933323849
734	1.150	1.1293341	1.12933323615
735	1.152	1.1293352	1.12933321520

* $n = \#$ of time-steps, $t = n \times 0.05$
† $Error$ = local error tolerance
Remark : Blow-up at $n \approx 735$

Energy Conservation - Table 3			
n*	$Error$† $= 10^{-5}$	10^{-9}	10^{-15}
0	$Energy = 1.119$	1.1192195	1.11921956057
10	1.119	1.1192195	1.11921956057
20	1.119	1.1192195	1.11921956057
30	1.119	1.1192196	1.11921956057
38	1.120	1.1192198	1.11921956058
39	1.120	1.1192199	1.11921956059
40	1.121	1.1192200	1.11921956062
41	1.121	1.1192202	1.11921956077

* $n = \#$ of time-steps, $t = n \times 0.05$

† $Error$ = local error tolerance

Remark : Blow-up at $n \approx 41$

Energy Conservation (BDF) - Table 4			
n*	$Error$† $= 10^{-5}$	10^{-9}	10^{-15}
0	$Energy = 1.119$	1.1192195	1.11921956057
10	1.119	1.1192195	1.11921956057
20	1.119	1.1192195	1.11921956057
30	1.119	1.1192196	1.11921956057
37	1.129	1.1192198	1.11921956058
40	1.120	1.1192201	
41	1.120	1.1192203	

* $n = \#$ of time-steps, $t = n \times 0.05$

† $Error$ = local error tolerance

Remark : Blow-up at $n \approx 41$

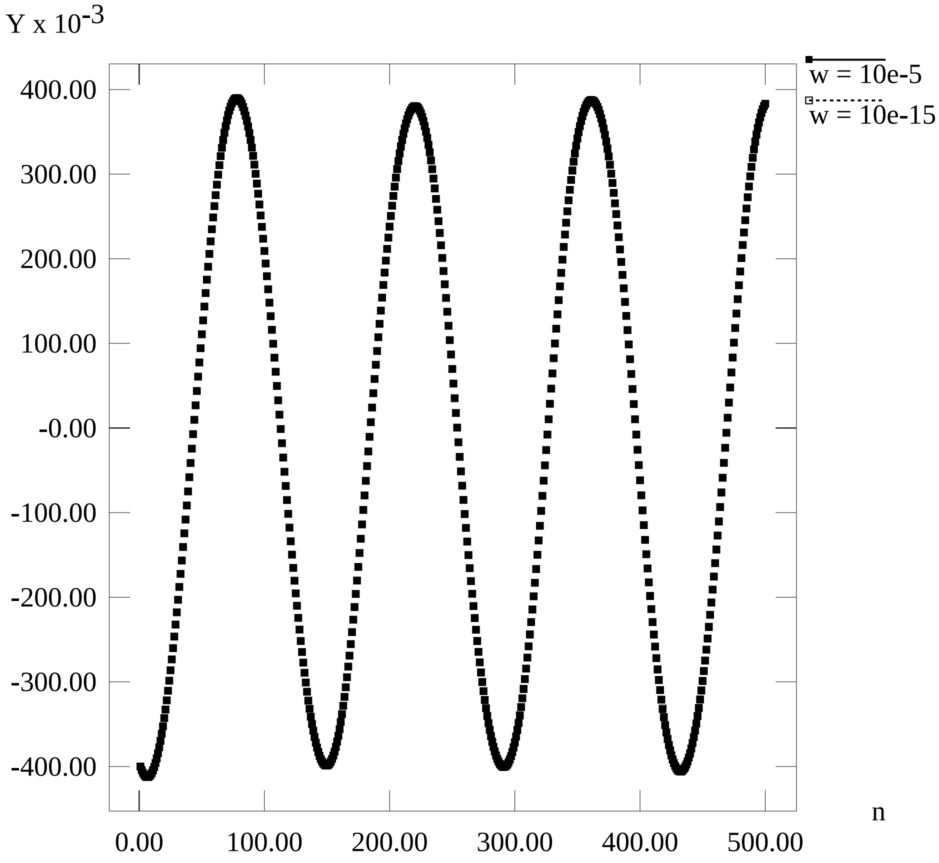
Y x 10-3
400.00
300.00
200.00
100.00
-0.00
-100.00
-200.00
-300.00
-400.00
w = 10e-5
w = 10e-15
n
0.00
100.00
200.00
300.00
400.00
500.00

Figure 1a

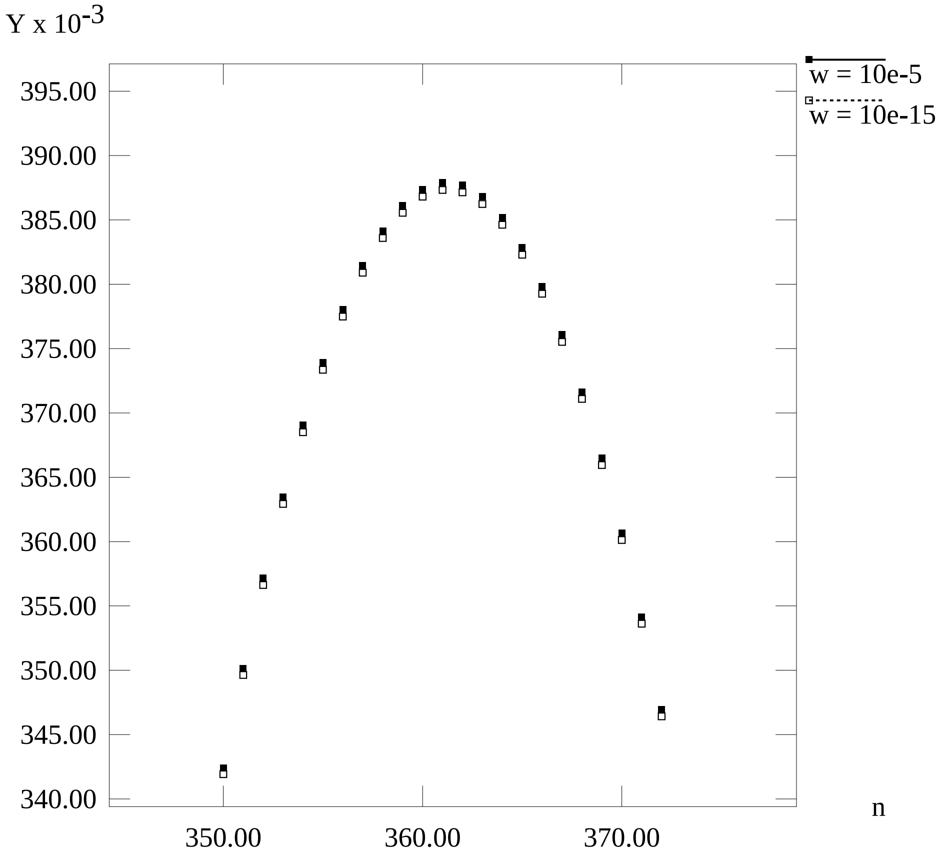
Y x 10-3
395.00
390.00
385.00
380.00
375.00
370.00
365.00
360.00
355.00
350.00
345.00
340.00
350.00
360.00
370.00
n
w = 10e-5
w = 10e-15

Figure 1b

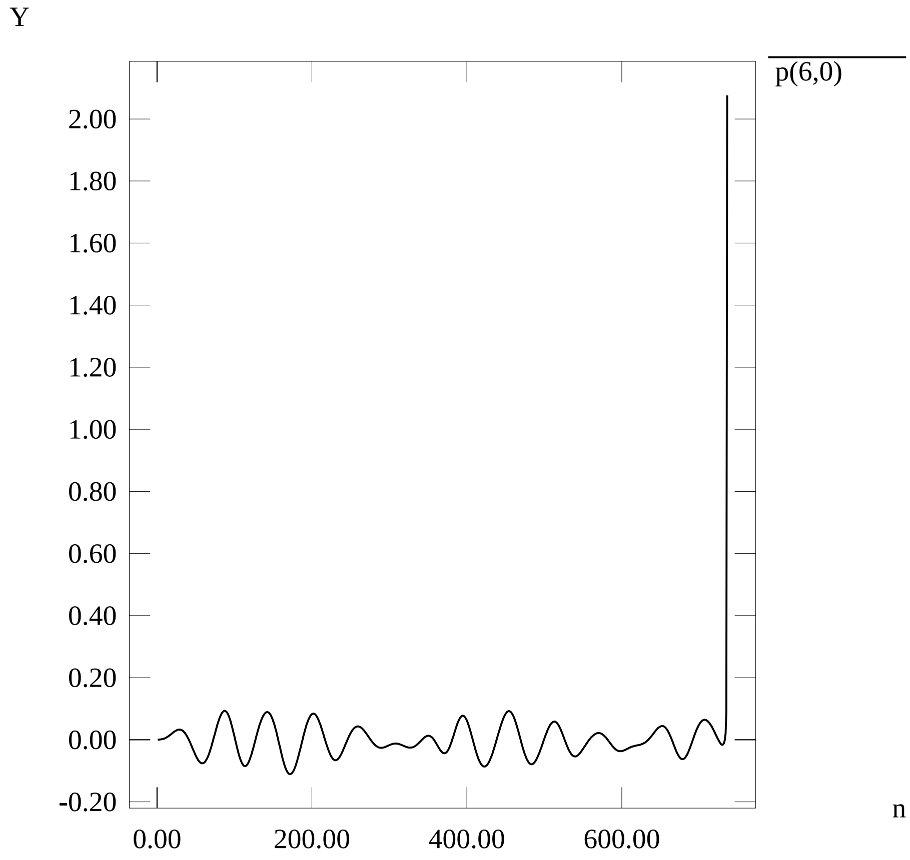
Y
p(6,0)
2.00
1.80
1.60
1.40
1.20
1.00
0.80
0.60
0.40
0.20
0.00
-0.20
0.00
200.00
400.00
600.00
n

Figure 2a

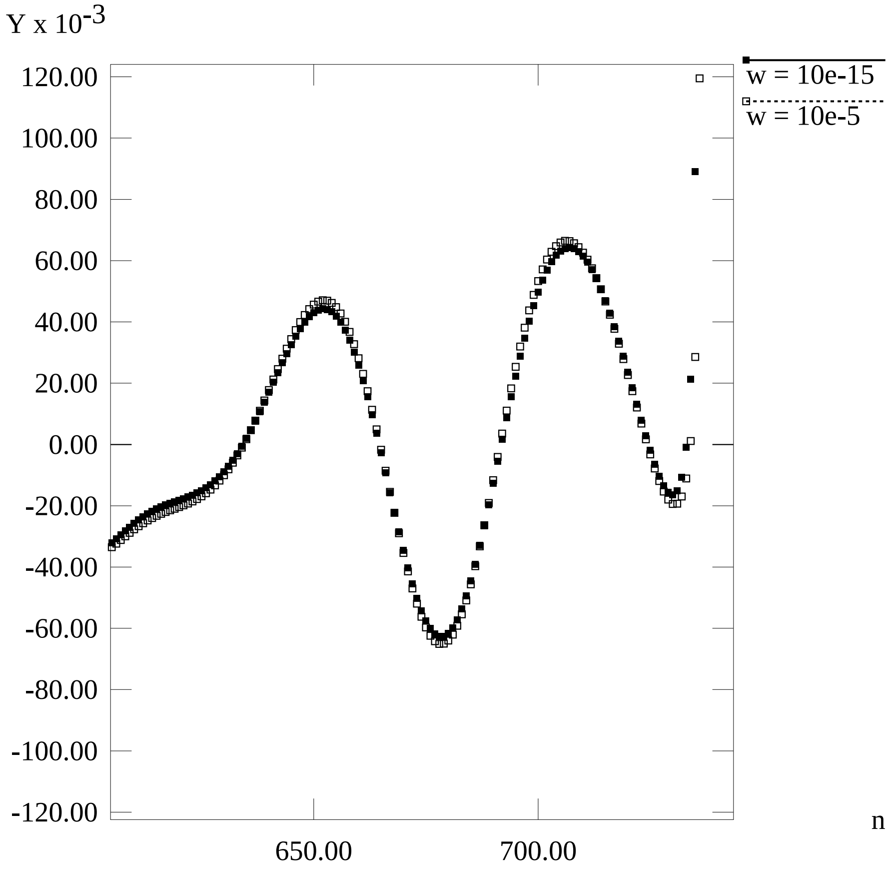
Y x 10-3
120.00
100.00
80.00
60.00
40.00
20.00
0.00
-20.00
-40.00
-60.00
-80.00
-100.00
-120.00
650.00
700.00
n
w = 10e-15
w = 10e-5

Figure 2b

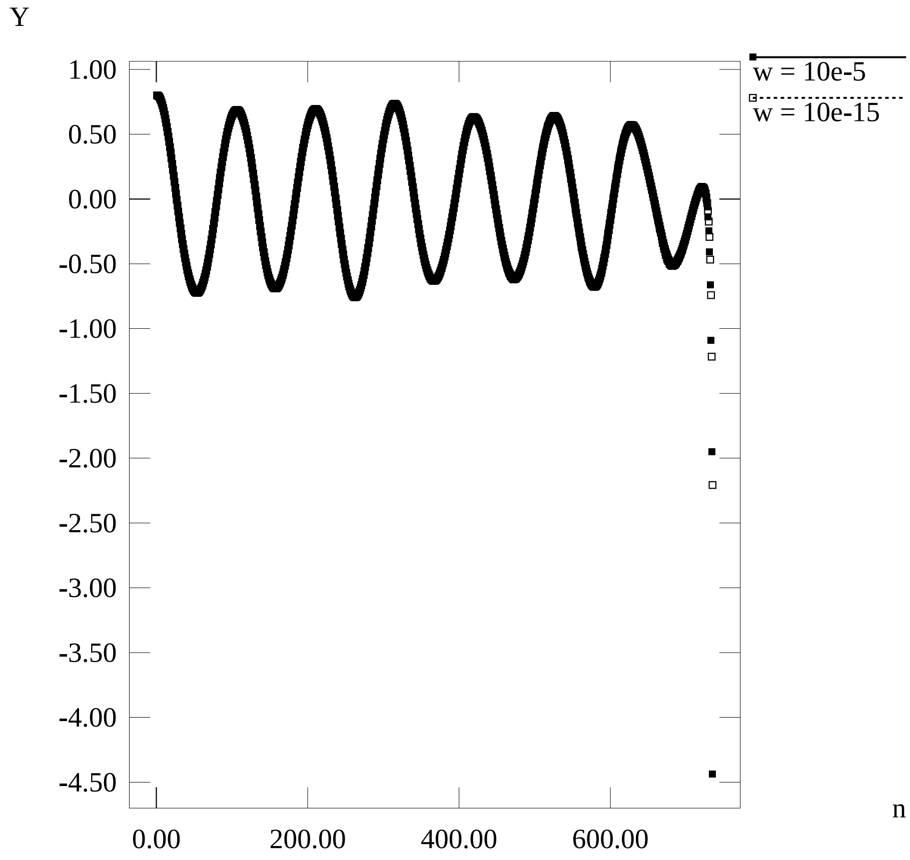
Y
1.00
0.50
0.00
-0.50
-1.00
-1.50
-2.00
-2.50
-3.00
-3.50
-4.00
-4.50
0.00
200.00
400.00
600.00
n
w = 10e-5
w = 10e-15

Figure 2c

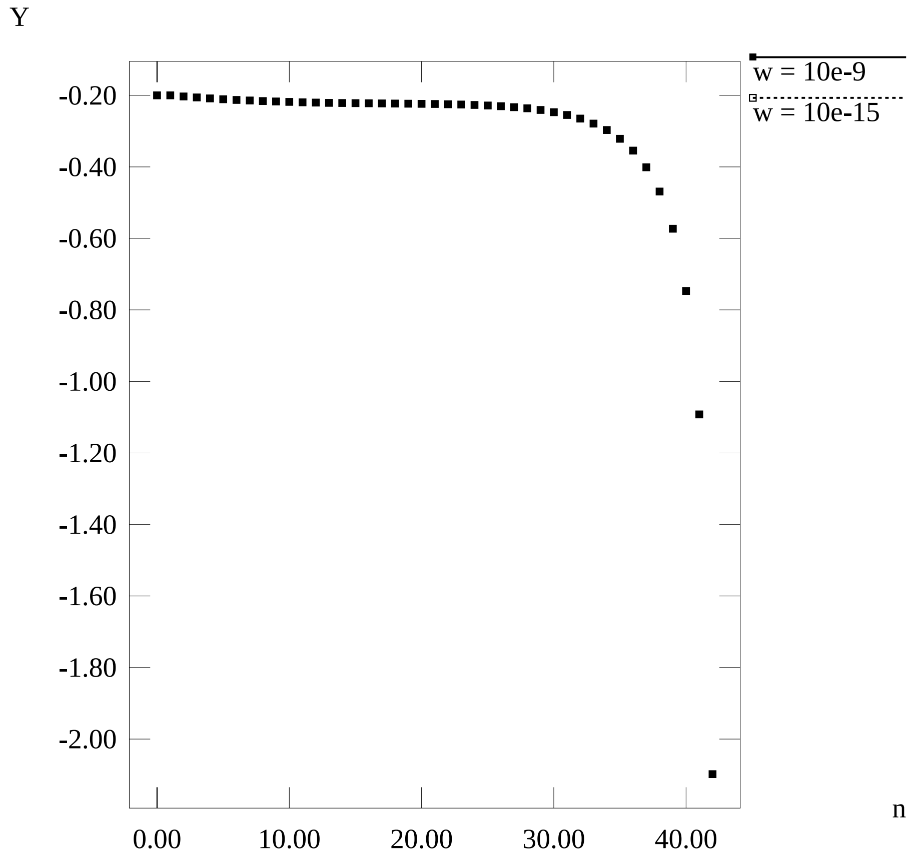

Y
-0.20
-0.40
-0.60
-0.80
-1.00
-1.20
-1.40
-1.60
-1.80
-2.00
0.00
10.00
20.00
30.00
40.00
n
w = 10e-9
w = 10e-15

Figure 3a

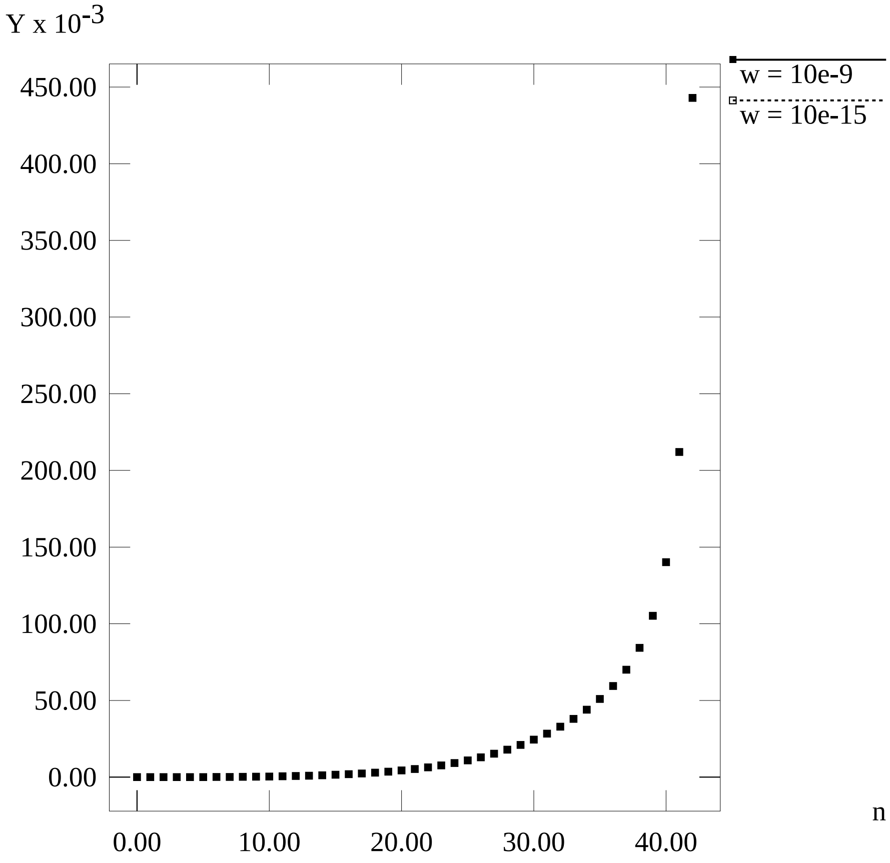
Y x 10-3
450.00
400.00
350.00
300.00
250.00
200.00
150.00
100.00
50.00
0.00
0.00
10.00
20.00
30.00
40.00
n
w = 10e-9
w = 10e-15

Figure 3b

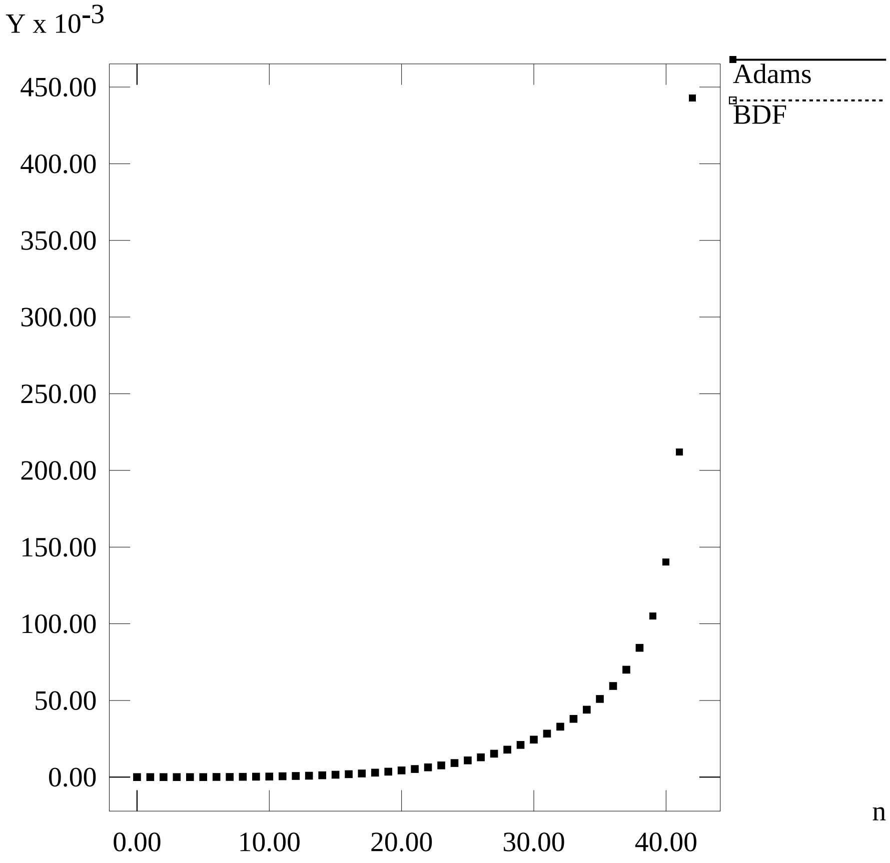

Y x 10-3
450.00
400.00
350.00
300.00
250.00
200.00
150.00
100.00
50.00
0.00
0.00
10.00
20.00
30.00
40.00
n
Adams
BDF

Figure 4

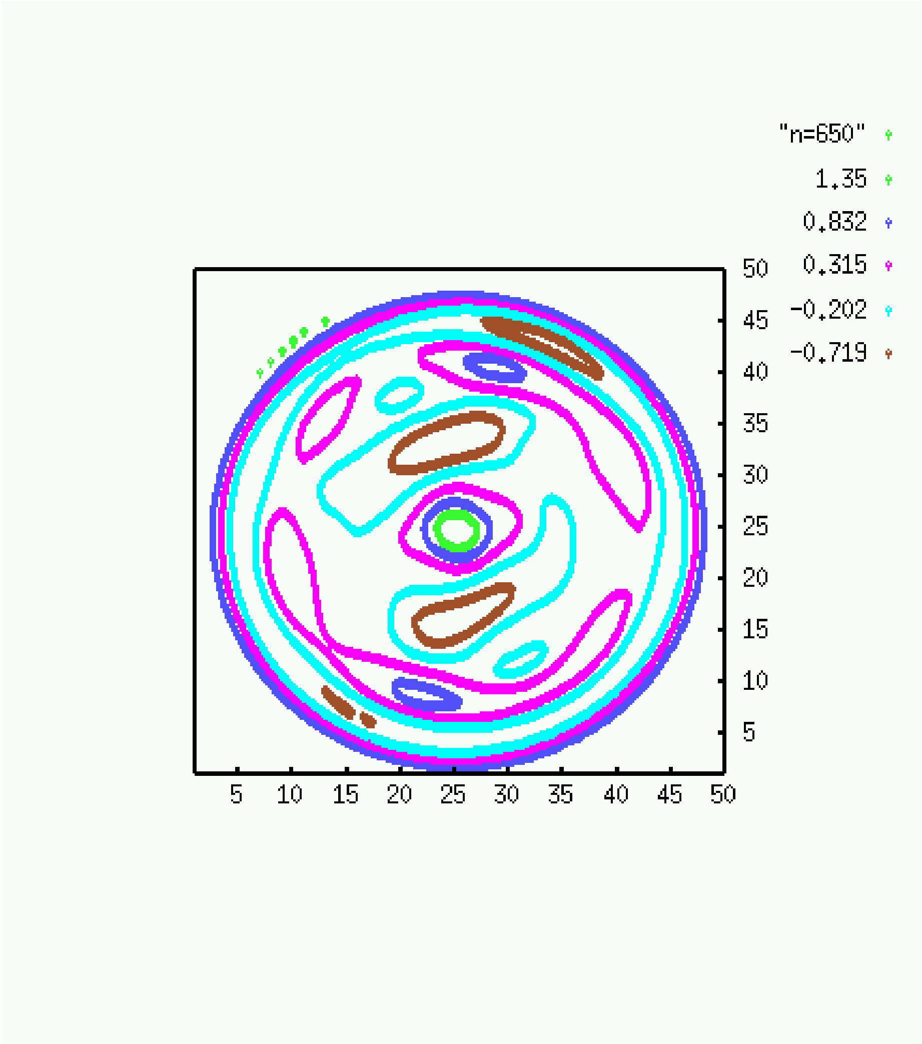
"n=650"
1.35
0.832
0.315
-0.202
-0.719
50
45
40
35
30
25
20
15
10
5
5
10
15
20
25
30
35
40
45
50

Figure 5a

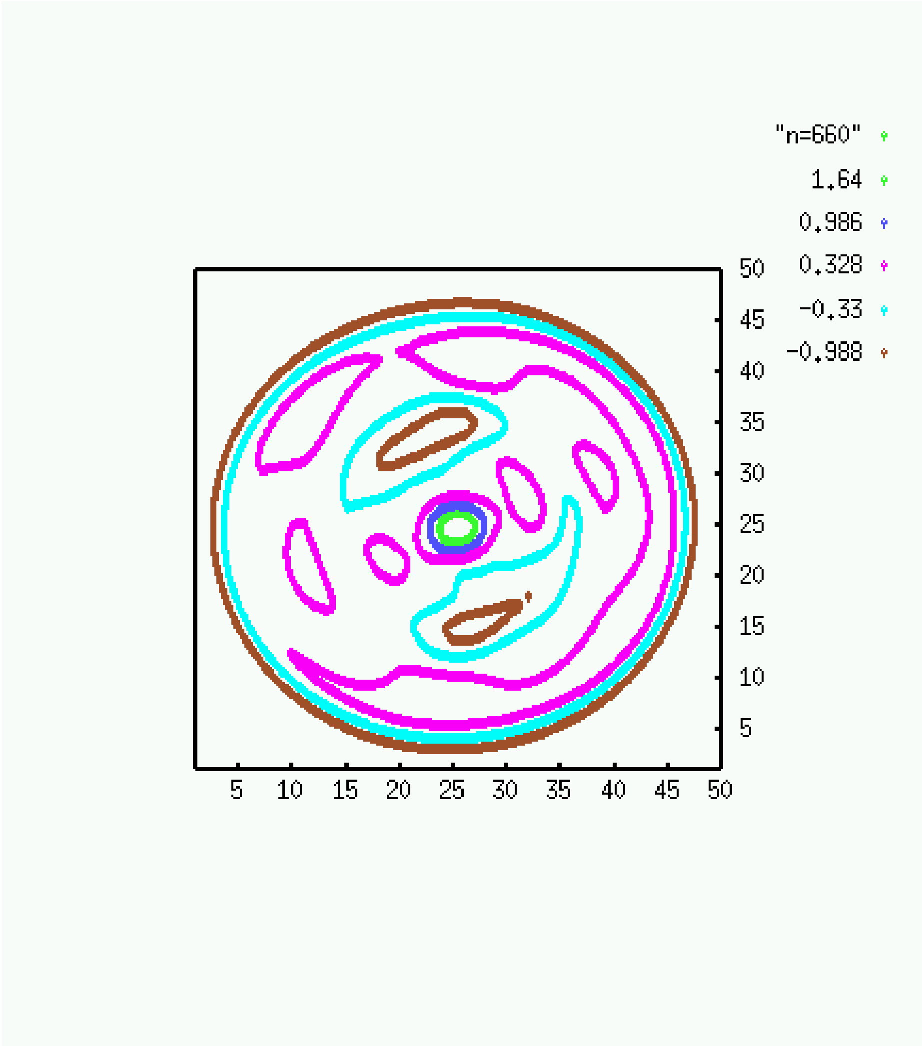

Figure 5b

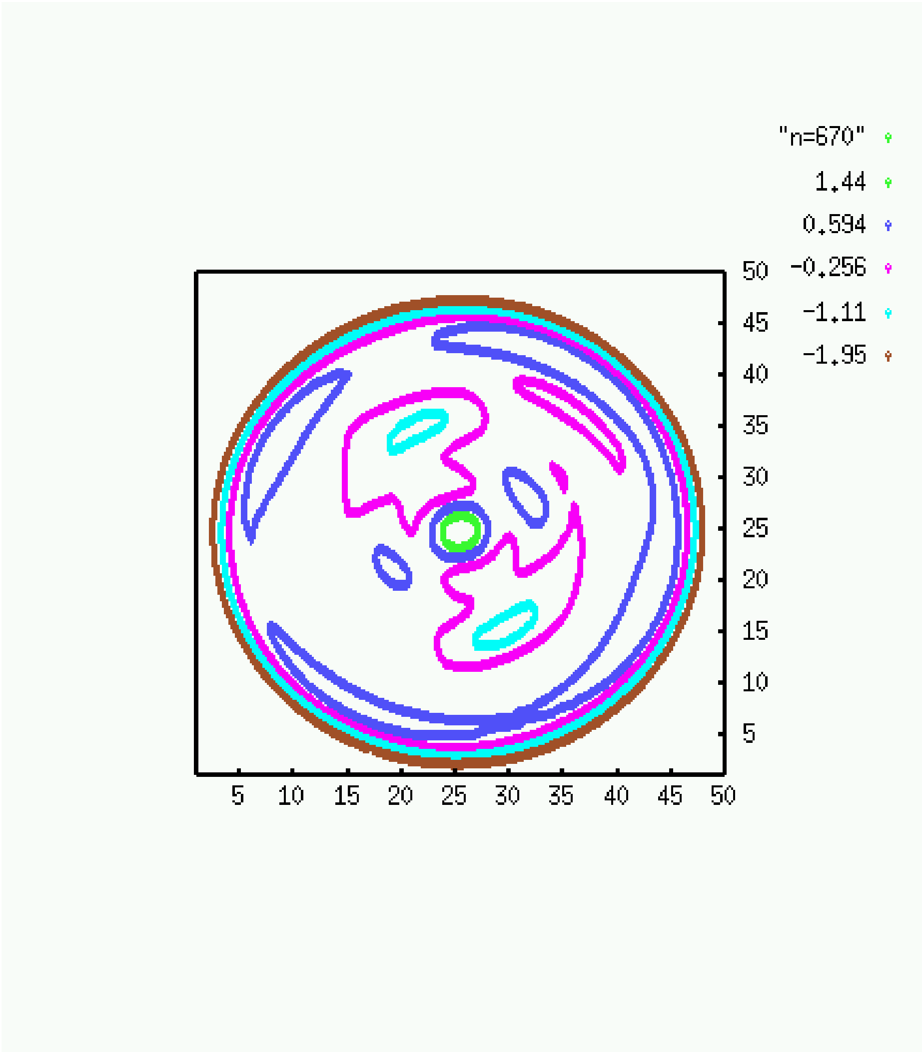
"n=670"
1.44
0.594
-0.256
-1.11
-1.95
5 10 15 20 25 30 35 40 45 50
5 10 15 20 25 30 35 40 45 50

Figure 5c

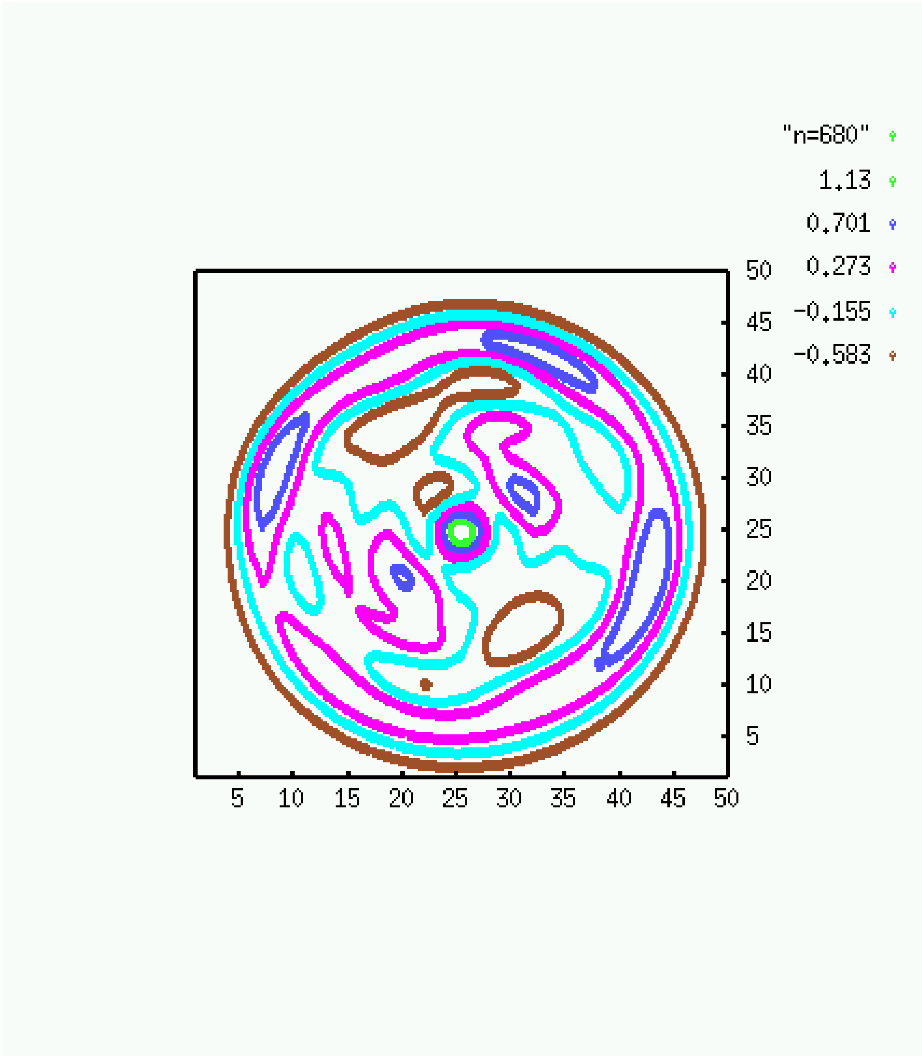
"n=680"
1.13
0.701
0.273
-0.155
-0.583
5
10
15
20
25
30
35
40
45
50
5
10
15
20
25
30
35
40
45
50

Figure 5d

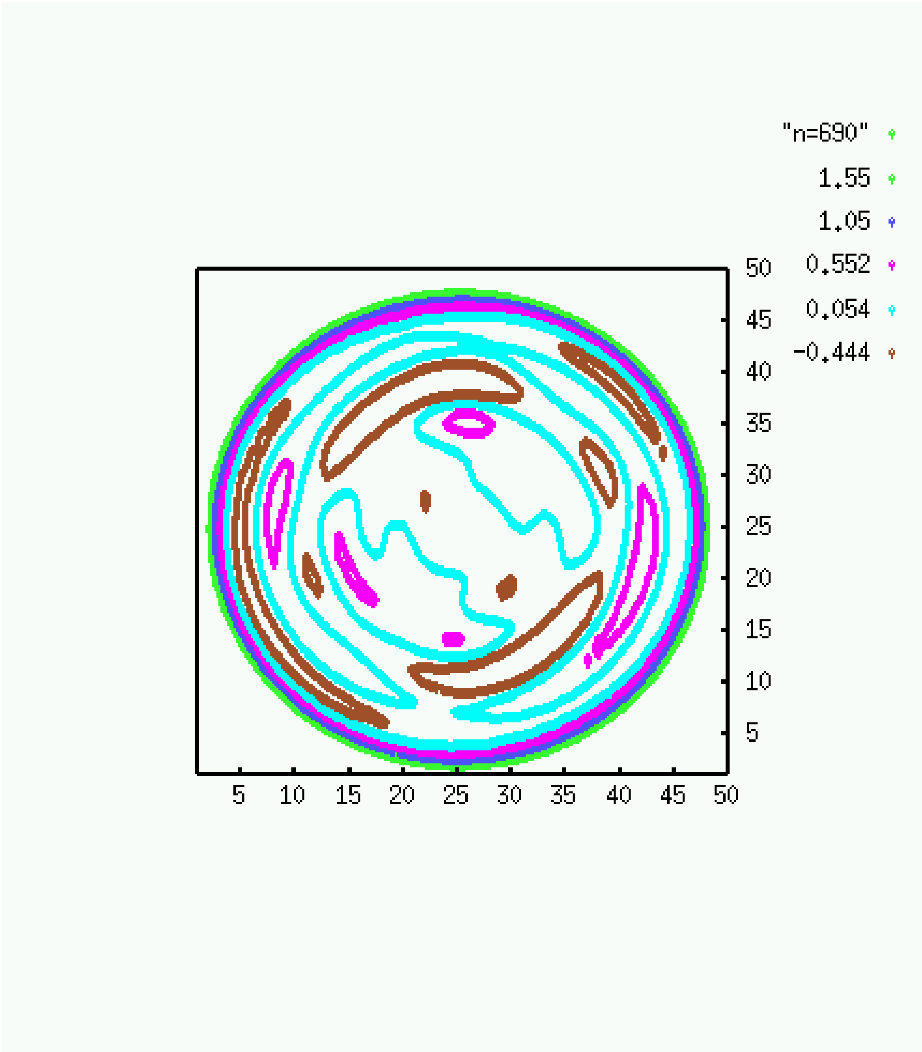
"n=690"
1.55
1.05
0.552
0.054
-0.444
50
45
40
35
30
25
20
15
10
5
5 10 15 20 25 30 35 40 45 50

Figure 5e

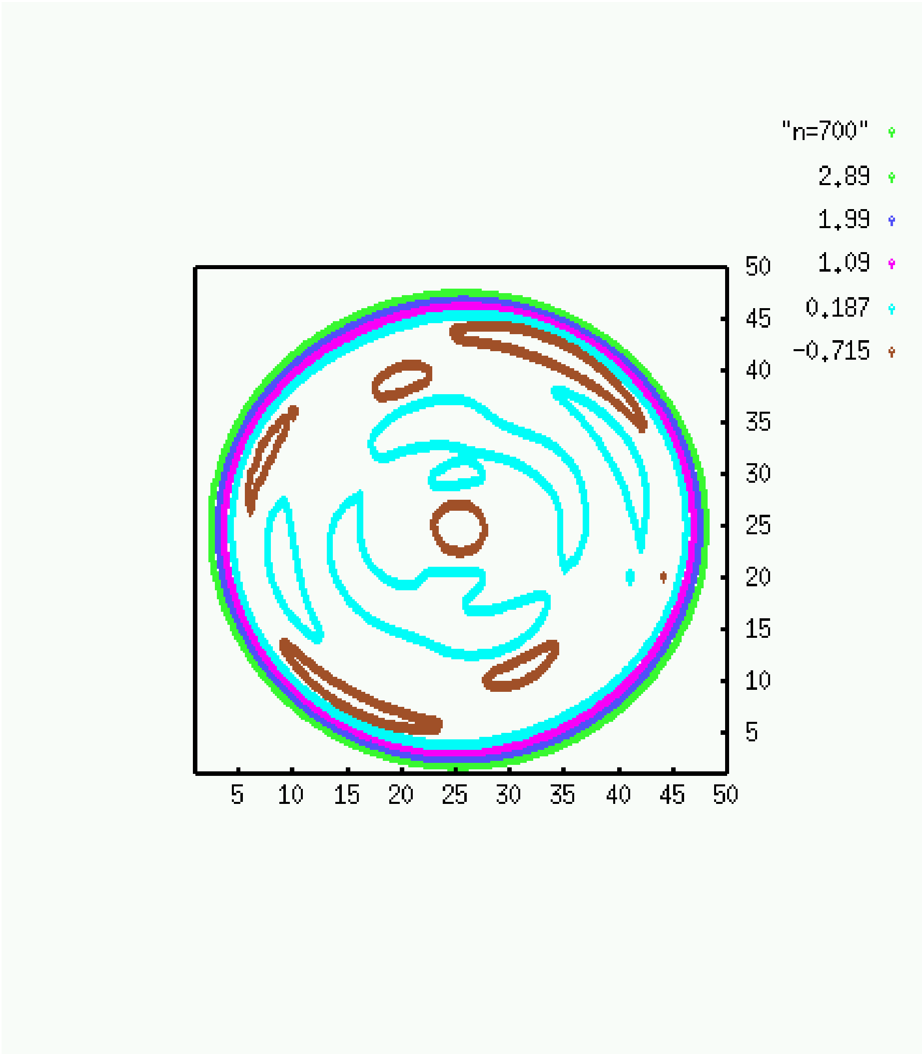
"n=700"
2.89
1.99
1.09
0.187
-0.715
50
45
40
35
30
25
20
15
10
5
5
10
15
20
25
30
35
40
45
50

Figure 5f

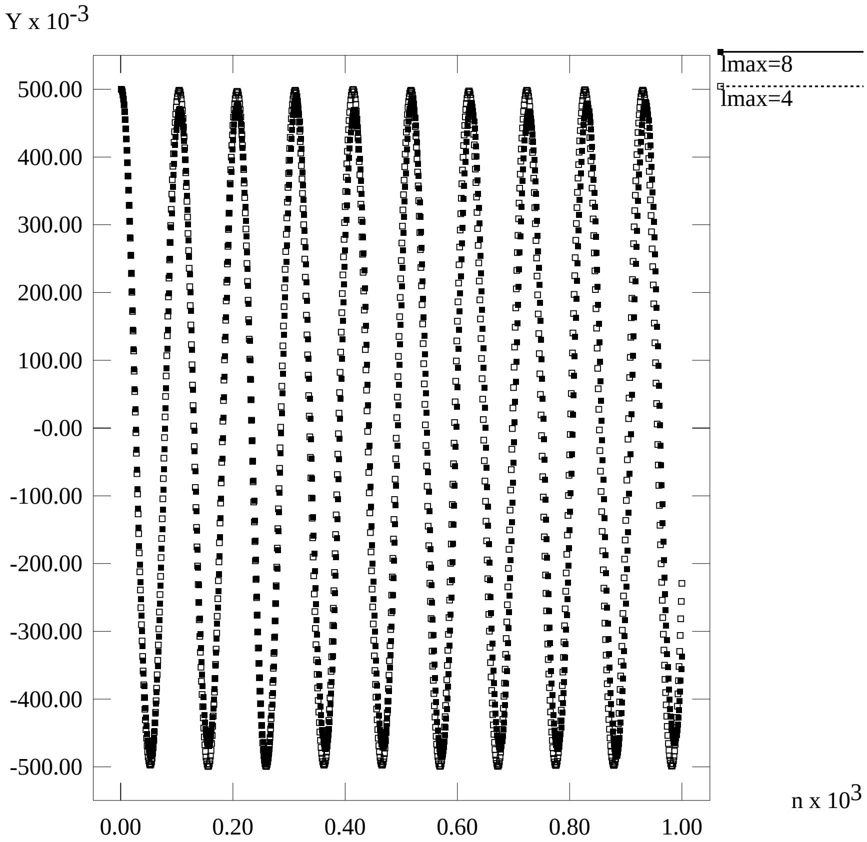
Y x 10-3
lmax=8
lmax=4
500.00
400.00
300.00
200.00
100.00
-0.00
-100.00
-200.00
-300.00
-400.00
-500.00
0.00
0.20
0.40
0.60
0.80
1.00
n x 103

Figure 6a

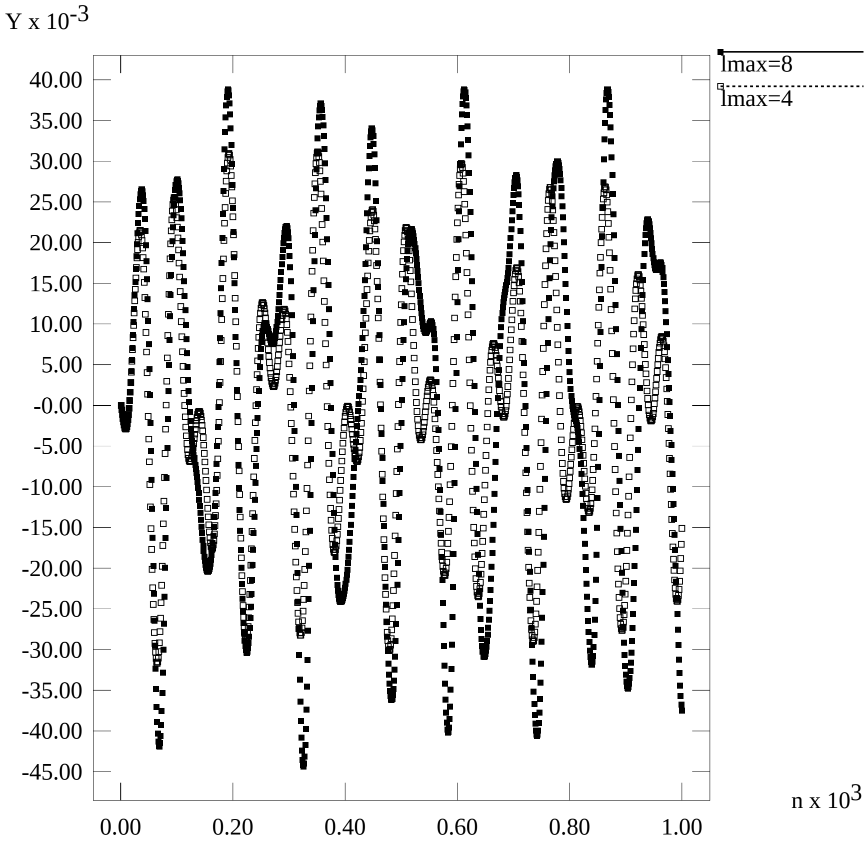
Y x 10-3
40.00
35.00
30.00
25.00
20.00
15.00
10.00
5.00
-0.00
-5.00
-10.00
-15.00
-20.00
-25.00
-30.00
-35.00
-40.00
-45.00
0.00
0.20
0.40
0.60
0.80
1.00
n x 103
lmax=8
lmax=4

Figure 6b

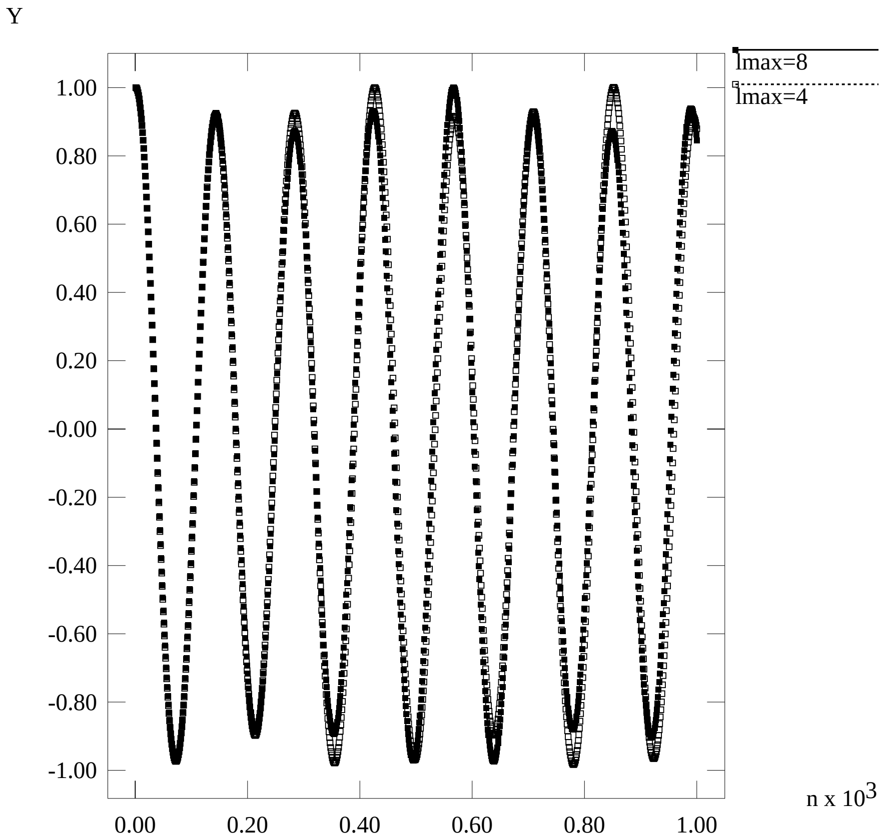
Y
lmax=8
lmax=4
1.00
0.80
0.60
0.40
0.20
-0.00
-0.20
-0.40
-0.60
-0.80
-1.00
0.00
0.20
0.40
0.60
0.80
1.00
n x 10^3

Figure 7a

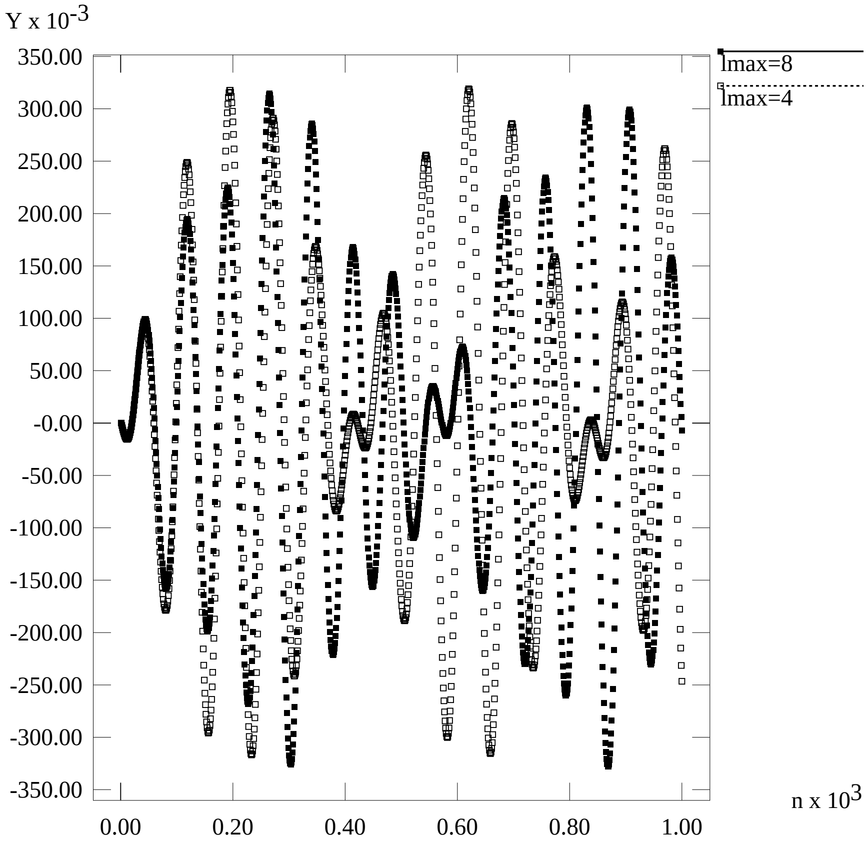
Y x 10-3
350.00
300.00
250.00
200.00
150.00
100.00
50.00
-0.00
-50.00
-100.00
-150.00
-200.00
-250.00
-300.00
-350.00
lmax=8
lmax=4
n x 103
0.00
0.20
0.40
0.60
0.80
1.00

Figure 7b